ELSEVIER

Materials Science and Engineering A270 (1999) 19–26

MATERIALS SCIENCE & ENGINEERING A

www.elsevier.com/locate/msea

Three dimensional atom probe investigation of vanadium nitride precipitates and the role of oxygen and boron in rapidly solidified 316 stainless steel

T.F. Kelly [a,*], D.J. Larson [b], M.K. Miller [b], J.E. Flinn [c]

[a] *Department of Materials Science and Engineering, 272 Materials Science and Engineering Building, University of Wisconsin, 1509 University Avenue, Madison, WI 53706, USA*

[b] *Metals and Ceramics Division, Oak Ridge National Laboratory, PO Box 2008, Oak Ridge, TN 37831-6376, USA*

[c] *Idaho Falls, ID 83415, USA*

Received 12 September 1998

Abstract

A 316 stainless steel that was rapid solidification processed (RSP) by gas atomization and hot extrusion of the powder has been studied previously by conventional atom probe field ion microscopy (APFIM). Vanadium, nitrogen, and oxygen have been introduced intentionally as alloying elements for the purpose of improving the mechanical properties through fine-scale precipitation. Previous efforts to locate the oxygen in the structure using APFIM were inconclusive, largely due to poor counting statistics. An energy-compensated three-dimensional position-sensitive atom probe (3DAP) has been used in the present study to search for oxygen in cavities, precipitates, and grain boundaries in this alloy. As a direct result of the much greater number of atoms detected and the three-dimensional imaging, oxygen concentrations on the order of 1 atomic% have been found both inside nitride precipitates and in the vicinity of grain boundaries. Boron was also found unexpectedly in concentrations of up to 2 atomic% inside nitride precipitates and in the vicinity of grain boundaries. These findings are important to developing an understanding of the grain growth resistance and precipitate stability both in this alloy and in this processing method in general.
© 1999 Published by Elsevier Science S.A. All rights reserved.

Keywords: Three dimensional atom probe; Rapid solidification processing; Stainless steel 316; Precipitation in stainless steel

1. Introduction

In a previous paper [1], it was shown that the mechanical properties of type 316 stainless steel can be markedly improved by rapid solidification processing (RSP) and aging of a vanadium-bearing variant of the standard alloy. This alloy and many other iron- and nickel-based gas atomized alloys have also shown extraordinary resistance to grain growth at elevated temperatures [2]. High nitrogen and oxygen contents were also intentionally introduced by melting under 80% nitrogen–20% oxygen gas and atomizing in nitrogen gas. On the order of 0.2 wt% of nitrogen can be entrained in stainless steel alloys during rapid solidification processing by this gas atomization approach [3]. As a result, a large number density ($\sim 2 \times 10^{21}$ m^{-3}) of 25 nm plate-like vanadium-rich nitrides precipitate during aging of the alloy [4] and these precipitates contribute to a major portion of the strengthening. It was also shown previously [5] that oxygen is an important alloying element in this processing approach. Our current understanding of the processing suggests that upon rapid solidification of the liquid, a high concentration of vacancies is produced in the solid which then condense to form a large number density of small cavities. Oxygen would stabilize the cavities against dissolution and these cavities serve as nucleation sites for the nitride precipitates. However, in the previous work where a conventional atom probe/field ion microscope (APFIM) was used, the distribution of the oxygen in the alloy was not determined due, in part, to poor counting statistics for oxygen. Because of the potential

* Corresponding author. Tel.: +1-608-2631073; fax: +1-608-2628353.

E-mail address: kelly@engr.wisc.edu (T.F. Kelly)

0921-5093/99/$ - see front matter © 1999 Published by Elsevier Science S.A. All rights reserved.
PII: S0921-5093(99)00239-7

for recording much higher total numbers of atoms from a given specimen volume, the use of a three-dimensional atom probe (3DAP) was suggested.

In the present work, which is a study of this same alloy in both the unaged and aged condition, an energy-compensated 3DAP is used to specifically look for oxygen in the structure as it might be distributed in cavities and precipitates, and at grain boundaries. Furthermore, a significant role for boron in the structure had not been considered in prior work. In this paper, statistically significant segregation of boron in the structure is found and this result has important ramifications for our understanding of the material. It has been difficult to explain the origin of the excellent grain growth resistance in gas atomized rapidly solidified alloys in terms of established theories of particle pinning because at least in the unaged condition, there are usually not enough particles present to maintain the small grain size. For this reason, evidence of any significant segregation to grain boundaries in these alloys is noteworthy and could help explain the grain growth resistance.

2. Experimental

A melt of 316 stainless steel with vanadium additions was atomized in nitrogen gas. Prior to atomization, the melt had been exposed to an 80% nitrogen–20% oxygen atmosphere. After sieving, the powder was hermetically sealed in carbon steel cans and extruded at 900°C at an extrusion ratio of 10:1. The specimen was then given a preconditioning heat treatment of 1100°C for 1 h followed by water quenching (the unaged condition). The nominal composition of the consolidated specimen was determined by inductively coupled plasma analysis and is shown in Table 1. This matrix composition shown in Table 1 was determined from the atom probe data in the unaged material from sections of the data that do not contain obvious segregation. Some specimens were subsequently aged at 600°C for 1000 h (the aged condition). In conventionally-processed 316 stainless steel, this aging treatment is about optimal for mechanical behavior. The RSP 316 Stainless steel has altered kinetics, however, and the optimal aging treatment has not been established.

In order to produce atom probe specimens, small rods ($1 \times 1 \times 10$ mm) were cut from the as-received specimen using a low speed diamond saw. The rods were prepared as sharp needles with a two-stage electropolishing technique at room temperature using 5 and 2% perchloric acid in glacial acetic acid at system voltages between 8 and 15 V.

APFIM studies were conducted at the Oak Ridge National Laboratory (ORNL) with a Kindbrisk Ltd. energy-compensated optical position-sensitive atom probe (ECOPoSAP). Field ion microscopy (FIM) was performed at a temperature of 60 K with 3×10^{-3} Pa of neon as the imaging gas. Atom probe analysis was performed at 4×10^{-9} Pa with a pulse fraction of 20% and a pulse repetition rate of 1500 Hz.

Table 1
Composition of the 316 stainless steel alloy of this study[a]

Element	Nominal composition (wt%)	Nominal composition (at%)	Matrix composition from unaged (at%)
B	–	–	$0.04 \pm -$
C	0.02	0.09	$0.08 \pm -$
N	0.19	0.75	0.45 ± 0.12
$N_{14}^{+} + Si_{28}^{++}$			1.99 ± 0.02
O	0.05	0.16	0.10 ± 0.01
Si	0.70	1.37	1.66 ± 0.12
$Si_{29}^{++} + Si_{30}^{++}$			0.13 ± 0.01
P	–	–	0.50 ± 0.01
V	0.65	0.70	0.60 ± 0.01
Cr	16.60	17.60	17.64 ± 0.07
Mn	1.60	1.61	1.87 ± 0.02
Fe	67.19	66.34	66.92 ± 0.08
Ni	10.70	10.05	8.61 ± 0.05
Cu	–	–	0.31 ± 0.01
Nb	–	–	$0.01 \pm -$
Mo	2.30	1.32	1.20 ± 0.02

[a] The nominal composition was determined by standard metallurgical analysis of a bulk specimen. A dash means that the value was not measured. The composition of the unaged specimen matrix of Fig. 1(c) is shown in the final column. A dash in the column means that the value is smaller than 0.01%. The error bars are calculated from number counting statistics ($\pm\sqrt{c(1-c)/N} = \pm\sqrt{n(N-n)/N}$) where $c = n/N$ is the composition, n is the number of atoms detected for a given element in an analysis and N is the total number of atoms detected in the analysis. The N and Si composition shown in the last column was determined from the $N_{14}^{+} + Si_{28}^{++}$ peak and the $Si_{29}^{++} + Si_{30}^{++}$ peak as described in the text.

There is an overlap between the N_{14}^{+}d $Si_{28}^{+\,+}$ peaks in the mass spectra. This overlap has been treated by showing the value of the entire peak at mass–charge ratio of 14. In most cases where the nitrogen concentration becomes large, this will represent primarily nitrogen. Furthermore, Si has isotopes of mass 29 (abundance = 4.7%) and mass 30 (abundance = 3.1%). In some cases, the value of these peaks is shown and these data provide an indication of the distribution of Si in the alloy. In Table 1, the N and Si compositions were determined by a simple deconvolution of the $N^{+}14 + Si_{28}^{+\,+}$ peak and the $Si_{29}^{+\,+} + Si_{30}^{+\,+}$ peak. Since the $Si_{29}^{+\,+} + Si_{30}^{+\,+}$ peak represents 7.8% of the Si statistically, then the total amount of silicon in the alloy should be $100/7.8 \times (Si_{29}^{+\,+} + Si_{30}^{+\,+}$ peak). Furthermore, the amount of N in the alloy should be $(N_{14}^{+} + Si_{28}^{+\,+}$ peak$) - 92.2/7.8 \times (Si_{29}^{+\,+} + Si_{30}^{+\,+}$ peak). Nitrogen is known to field evaporate in molecular species with a variety of metal atoms. Strong peaks were observed for $(V_{51}N_{14})^{+\,+}$, $(Cr_{52}N_{14})^{+\,+}$, and $(Fe_{56}N_{14})^{+\,+}$ and minor peaks for $(Mo_{92}N_{14})^{+\,+\,+}$, $(Nb_{93}N_{14})^{+\,+\,+}$, and $(Mo_{96}N_{14})^{+\,+\,+}$ were also present. In all of these cases, a nitrogen atom was counted and Fig. 2c reflects these nitrogen atoms though the legend does not explicitly call attention to them.

All composition data points are determined from 200 ion blocks. The B and O plots have been calculated with a four-period moving average to smooth the statistical fluctuations. This smoothing function takes the current data value in a series and adds to it the three (four minus one) previous data values and divides by four to arrive at a moving average value.

3. Results

3.1. Unaged RSP 316 stainless steel

As shown in Fig. 1, a FIM specimen (Fig. 1a) of the unaged 316 SS was prepared with a grain boundary along its shank. There is also a transverse grain boundary very near the apex. The intersection of this longitudinal grain boundary with the apex surface of the tip can be seen in the FIM image of this tip, Fig. 1b. This FIM image was recorded after the 3DAP analysis shown in Fig. 1c, which is a projection down the z-axis. The image in Fig. 1c has an original size of about $15 \times 15 \times 26$ nm for the X, Y, and Z dimensions, respectively. The matrix composition presented in Table 1 closely matches the nominal composition of the alloy. However, the corrected N composition of the matrix is slightly high and the corrected Si composition is slightly low. It appears that the simple correction used for the N/Si peak overlap based on the $Si_{29}^{+\,+} + Si_{30}^{+\,+}$ peak overcompensates.

The FIM image shows a line of brightly imaging atoms across it. This feature is presumed to be the longitudinal grain boundary evident in the TEM image, Fig. 1a. Within the volume of the 3DAP image, Fig. 1c, no sensible segregation was found for any of the substitutional elements in the alloy. There was no segregation of phosphorus or carbon observed. However, Fig. 1c does show clear evidence of segregation of both boron and oxygen. The boron is segregated to the upper right corner of the projected image. In a 3D rendering of the image it is clear that this trend of boron segregation to the $X \approx 0$, $Y \approx$ large corner holds throughout the volume. Oxygen is segregated to a different location in the image: $X \approx 1/2$, $Y \approx 2/3$ and this trend also holds throughout the volume. It is not obvious why these elements have segregated to these locations and the 3D image does not provide structural information that can bear on this question. The apparent location of the grain boundary in the FIM image at the end of the analysis does correspond, at least in part, to the location of the oxygen concentration maximum. Though it is not possible to say definitively that the elevated concentrations of either boron or oxygen in Fig. 1c and d correspond precisely to the known location of the grain boundary, it does appear that both of these concentration maxima occur within 10 nm of the grain boundary.

The FIM images obtained prior to initiation of the 3DAP analysis showed no feature that could be interpreted as a grain boundary and very little material was removed from the tip shown in Fig. 1a prior to the 3DAP analysis. The 3DAP analysis that was performed was expected to pass through the transverse boundary and evidence of the transverse grain boundary was expected in the 3DAP image in some form. Unfortunately, the tip flashed just after the Fig. 1b was recorded which precluded further observation of the tip in the TEM. As a result, it is not clear from the data where the grain boundary was located during the acquisition of the 3DAP image.

It is also worth noting that the maxima in the boron and oxygen concentrations occur at different locations. In fact, it appears that these two elements countersegregate. The composition profile in Fig. 1d was extracted from the region shown in Fig. 1c and it shows an oxygen concentration maximum where the boron concentration is very low at about 10 nm on the distance scale. Similarly, the boron concentration is maximum, And approaches 1 atomic%, from 18 to 20 nm on the distance scale where the oxygen concentration is low.

3.2. Aged RSP 316 stainless steel

A TEM image of a FIM specimen of aged 316 SS is shown in Fig. 2a. The FIM image in Fig. 2b shows a brightly imaging precipitate centered in the analysis

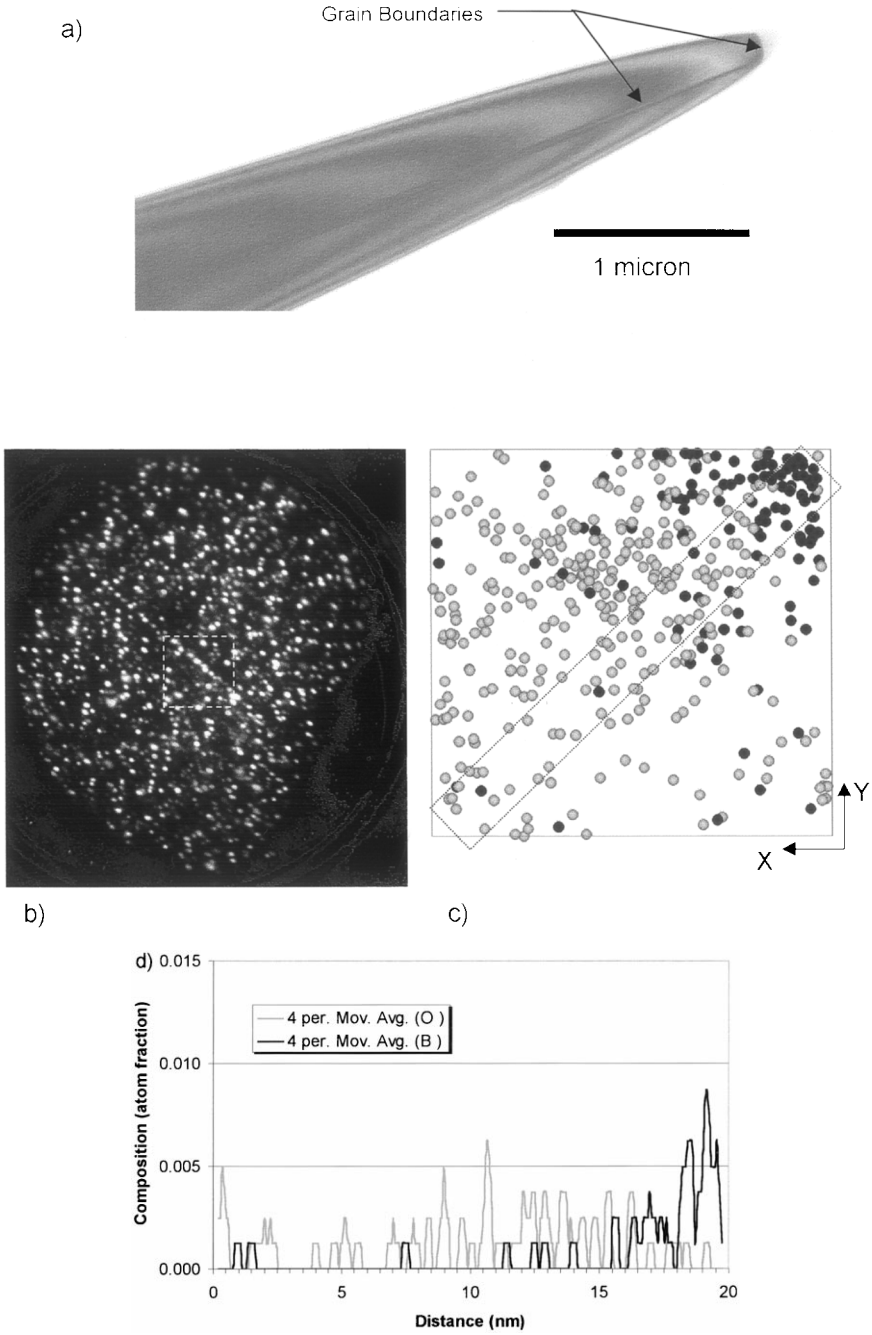

Fig. 1. (a) TEM Image of an APFIM specimen of unaged 316 SS; (b) FIM image of the tip in (a) at the end of the 3DAP analysis. The inset square marks the region of the 3DAP analysis; (c) 3DAP image of the tip in (a) above showing only oxygen (light) and boron (dark) atoms. This image is 15 × 15 × 26 nm and is projected along the latter direction; (d) composition profile of oxygen and boron based on 200 atom blocks along the dashed box in (c) from lower left to upper right. The plotted profile is determined by a moving average over four periods (see text).

region. The DAP image shown in Fig. 2c–g clearly shows the presence of the precipitate. This precipitate is a vanadium-rich metal nitride with a nominal composition of (see Fig. 2h) 30 at% Cr; 23 at% V; 2 at% Ni; 18 at% N; balance Fe which is consistent with the type I nitride in our previous work with a conventional APFIM [1]. Note that the nitrogen concentration in the matrix away from the precipitate in Fig. 2h reaches about 3%. This value is likely artificially high by about 1.5–2% due to the inclusion of Si in the N data. The Si 3DAP image, Fig. 2g, illustrates that the Si concentration as determined by the Si_{29}^{++} and Si_{30}^{++} peaks is reduced in the precipitate relative to the matrix. This supports the notion that the N concentration determined in the precipitate is not strongly influenced by the Si concentration but the matrix concentration of N is influenced.

A significant concentration of both boron and oxygen are found in this image. A composition profile was derived from the 3DAP image by integrating the composition along the arrow shown in Fig. 2c. The result is shown in Fig. 2h and i. Note that both the boron concentration in the precipitate (about 1.5 at%) and the oxygen concentration in the precipitate (about 0.9 at%) are elevated relative to the global concentrations in the alloy, Table 1. Furthermore, the boron concentration is elevated outside the precipitate as illustrated in the composition profile, Fig. 2i, at a distance of about 9–12 nm. In this latter case, the oxygen concentration is again low when the boron concentration is high.

Fig. 3 shows another profile of boron and oxygen concentrations taken from the same 3DAP image in Fig. 2 but in a direction starting in the precipitate and moving toward the region of high boron concentration in Fig. 2f. It shows a high boron concentration again away from the precipitate. The vanadium concentration is also shown as a way to illustrate the spatial extent of the precipitate. In this case, the boron concentration reaches 2 at% and again the oxygen concentration is low when the boron concentration is high.

4. Discussion

Perhaps the most outstanding novel characteristic of rapidly solidified gas-atomized metals over the past two decades has been their microstructural stability. Not only is the grain growth at elevated temperatures greatly diminished, but also the creep stability and

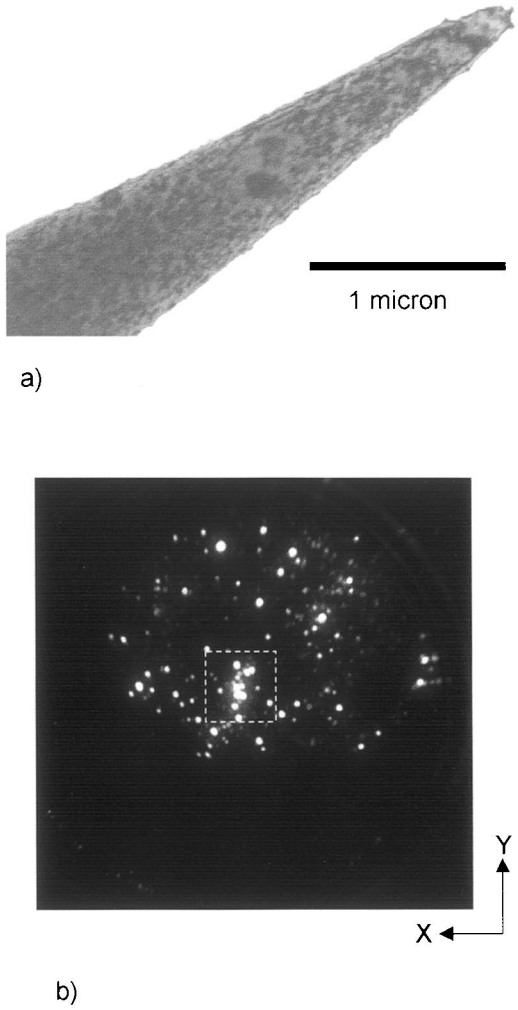

Fig. 2. (a) TEM Image of an APFIM specimen of aged 316 SS; (b) FIM image of the tip in (a) that shows a brightly imaging nitride precipitate prior to 3DAP analysis. The inset square marks the region of the 3DAP analysis. (c–g) 3DAP images of the Fe, V, O, B and $Si_{29} + Si_{30}$ atoms, respectively. The arrow in (c) shows the direction of the composition profile (below) through the precipitate; (h) composition profile of Cr, V, and $(N + Si_{28})$ based on 200 atom blocks through the precipitate; (i) composition profile of O and B based on 200 atom blocks through the precipitate. The plotted profile is determined by a moving average over four periods (see text). The rectangular parallelepiped volume over which the composition profile is integrated is 12 nm in the direction of the arrow and 8×8 nm in cross-section.

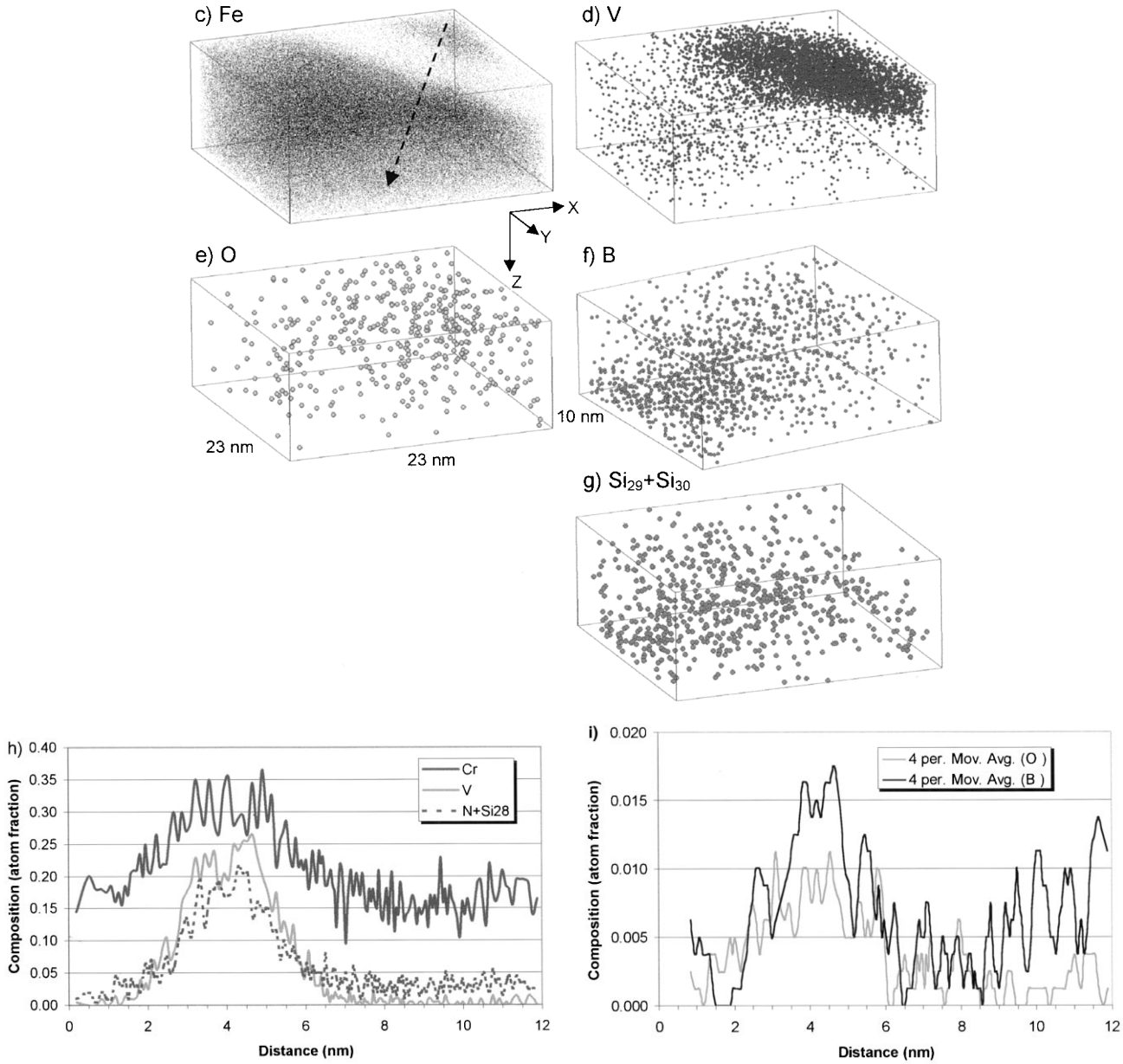

Fig. 2. (*Continued*)

precipitate stability is typically much enhanced. In searching for a common explanation for these related phenomena, there appears a plausible, but nebulous argument that there is some compositional effect that results from the rapid solidification/gas atomization that does not result from conventional ingot metallurgy. The observation of stable cavities has suggested that oxygen may play a role and indeed there has been experimental data that corroborates this notion [6]. However, nothing concrete to this point has suggested that boron is in any way involved in stabilization of the microstructure. Indeed. with a conventional atom probe in our previous work, there was no statistically significant finding of enrichment of either boron or oxygen. With the much greater amount of data that is generated with a 3DAP, it is possible to make observations that are statistically meaningful for both of these impurity elements in the steel.

Boron concentrations at grain boundaries have been found to be especially effective in stabilizing the grain structure of nickel aluminide [7,8]. Boron segregation to grain boundaries in these materials has been linked to a greatly enhanced grain coarsening resistance and creep resistance. Boron has also been observed to stabilize the grain structure in steels [9,10]. In each of these cases, an atom probe was used to detect the boron at the grain boundary. In fact, in a recent study [10], 1at% of B was found at the grain boundaries in a steel that exhibited exceptional grain

stability. This is essentially the same value that was detected in the present work at several locations in the structure.

It is also noteworthy that boron is found in similar concentrations in the nitride precipitates in this steel. The effect of the boron on the stability of the nitrides is not known but it is known that these nitrides resist coarsening and dissolution to higher temperatures than nitrides nitrides in similar conventionally-processed steels.

Boron has been found by several investigators to be subject to trajectory aberrations in atom probe analysis [11–13]. The boron appears to be 'sprayed' away from the boundary location by local distortions in the field created by local deviations from a smooth surface at the boundary. Similar effects should occur around a precipitate. This effect is most prominent for light elements and so should affect the oxygen distribution as well. The fact that the boron is found at elevated concentrations near a grain boundary but not on the grain boundary could be due to this effect. However, it would be difficult to explain the apparent observation of countersegregation of oxygen and boron (see next paragraph) if this mechanism plays a role, especially when both countersegregation and cosegregation occur simultaneously at the precipitates.

So what is the role of oxygen? There appear to be two trends relative to the boron distribution in the material. In the matrix of this steel, boron and oxygen appear to counter-segregate, that is, where boron is found in higher concentrations, low concentrations of oxygen are not found and vice versa. Oxygen may still play a crucial role in stabilizing the microstructure in a manner similar to that of boron. However. the added complexity of counter-segregation of these two elements may even enhance the effect of each element on their own. If changes to the microstructure require changes in the distribution of these elements, then both elements would need to be redistributed and that would be much more difficult to accomplish than the case of a single element For example, these elements may have formed atmospheres about a defect. This is consistent with our observations. In order for the defect to move, both oxygen and boron would have to move in such a way that they avoid each other.

Given this behavior in the matrix, it is curious to find both oxygen and boron at elevated concentrations simultaneously inside the precipitates. Clearly the thermodynamics of their interaction is different between the matrix and the precipitate.

In our previous work [1], it was noted that small (2–4 nm) cavities were found in the unaged material. These cavities are thought to be stabilized by oxygen or an oxide film coating them [14]. Furthermore, these fine-scale cavities are found to be directly associated with the precipitates which form during aging and appear to serve as nucleation sites [6]. The oxygen found inside the precipitates might be due to the prior presence of an oxygen-coated cavity, however, there is insufficient direct evidence to conclude this unequivocally. Furthermore, cavities were not obvious in the several FIM specimens of unaged material that were examined in the present study. It is often the case. however, that the observation of cavities is not uniform in a structure and it is necessary to search sometimes over an area to find them in a TEM specimen. This effect may be due to the fact that these are powder-processed materials and there is a different solidification history in each powder particle. Not all particles achieve the high liquid supercooling that is necessary for cavity formation. This apparently contradictory finding with previous observations may be due to this effect and the fact the volume of material examined in a FIM specimen is very small compared with the volume of examined material in a TEM specimen.

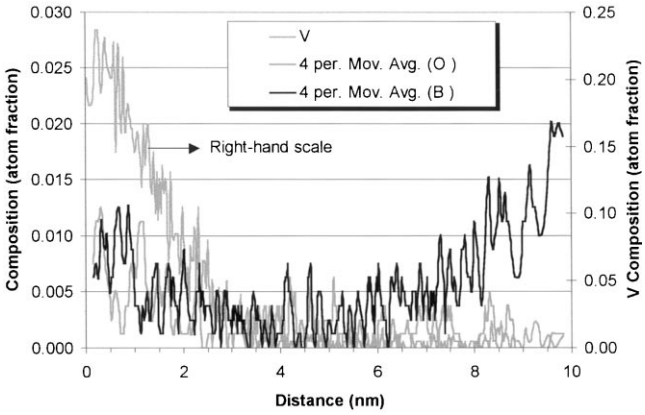

Fig. 3. Composition profile from inside the precipitate to the far side of the 3DAP image in Fig. 2. The V composition is plotted on the right-hand scale and illustrates the location of the transition from precipitate to matrix composition. The plotted profiles for oxygen and boron are determined by a moving average over four periods (see text).

5. Conclusions

- Oxygen is segregated to elevated concentrations in both the nitride precipitates of the aged material and to the vicinity (within 10 nm) of a grain boundary in the unaged material.
- Boron also is segregated to elevated concentrations in both the nitride precipitates of the aged material and to the vicinity (within 10 nm) of a grain boundary in the unaged material.
- Oxygen and boron co-segregate to the nitride precipitates of the aged material. These two elements, however, are found to be countersegregated in the matrix near a grain boundary of the unaged material.
- The oxygen and boron concentrations in the nitride precipitates is on the order of 1 at% and this fact may be responsible for their enhanced thermody-

namic stability relative to nitrides in similar conventionally-processed alloys.

- The relatively large intercepted volume of the 3DAP makes it possible to make observations concerning elements at very low concentrations that would not be discernable in a conventional APFIM.

Acknowledgements

This research was sponsored in part by the Division of Materials Sciences, US Department of Energy, under contract DE-AC05-96OR22464 with Lockheed Martin Energy Research Corp. and through the SHaRE Program under contract DE-AC05-760R00033 with Oak Ridge Associated Universities, and by an appointment (DJL) to the ORNL Postdoctoral Research Associates Program administered jointly by the Oak Ridge Institute for Science and Education and ORNL. This research was conducted, in part, utilizing the Shared Research Equipment User Program facilities at Oak Ridge National Laboratory. A portion of this work was performed at the Materials Science Center of the University of Wisconsin (UW), which receives partial support from the NSF-Materials Research Science and Engineering Center (MRSEC) at the UW.

References

[1] S. Wisutmethangoon, T.F. Kelly, J.E. Flinn, P.P. Camus, D.J. Larson, M.K. Miller, Mats. Sci. Eng. A 250 (1998) 43.
[2] M. Cohen, B.H. Kear, R. Mehrabian, Rapid Solidification Processing, in: R. Mehrabian, B.H. Kear, M. Cohen (Eds.), Principles and Technologies II, Claitors Publishing Division, Baton Rouge, 1980.
[3] J.E. Flinn (1996) unpublished research.
[4] L.E. Collins, Can. Met. Quarterly 25 (1) (1986) 59.
[5] J.E. Flinn, T.F. Kelly, US Patent number 08/638,080, April (1996).
[6] T.F. Kelly, K. Shin, J.C. Bae, R.K. Noll, J.E. Flinn, High-Resolution Electron Microscopy of Defects in Materials, U. Dahmen, R. Sinclair, D.J. Smith (Eds.), Materials Research Society (1990). Also T.F. Kelly, J.E. Flinn, J.C. Bae, unpublished research.
[7] M.K. Miller, D.J. Larson, K.F. Russell, Characterization of Segregation in Nickel and Titanium Aluminides, in: M.V. Nathal, R. Darolia, C.T. Liu, P.L. Martin, D.B. Miracle, R. Wagner, M. Yamaguchi (Eds.), Structural Intermetallics, TMS, Warrendale, PA, 1997, p. 53.
[8] D.J. Larson, M.K. Miller, Atom Probe Field Ion Microscopy Characterization of Nickel and Titanium Aluminides, Mats. Char. (1999), in press.
[9] L. Karlsson, H. Nordén, Acta Metall. 36 (1988) 13.
[10] K. Seto, D.J. Larson, P.J. Warren, G.D.W. Smith, Scripta Mat., (1998), in press.
[11] R. Waugh, Southon, Surf. Sci. 68 (1977) 79–85.
[12] R. Waugh, Southon, Surf. Sci., 89, (1979) 718–724.
[13] M. Thuvander, M.K. Miller, (1998) unpublished research.
[14] S. Zinkle, L.E. Seitzman, W.G. Wolfer, Phil. Mag. A 55 (1) (1987) 127.